Sinking particle export within and beneath the euphotic zone in the eastern Indian Ocean

Michael R. Stukel [a,b,*] , Tristan Biard [c], Moira Décima [d], Christian K. Fender [a], Opeyemi Kehinde [a], Thomas B. Kelly [e], Sven A. Kranz [f], Manon Laget [c], Michael R. Landry [d], Natalia Yingling [a]

[a] *Dept. of Earth, Ocean, and Atmospheric Science, Florida State University, Tallahassee, FL, 32306, USA*
[b] *Center for Ocean Atmospheric Prediction Studies, Florida State University, Tallahassee, FL, 32306, USA*
[c] *Laboratoire d'Océanologie et de Géosciences, Univ. Littoral Côte d'Opale, Univ. Lille, CNRS, IRD, UMR, Wimereux, 8187, France*
[d] *Scripps Institution of Oceanography, University of California San Diego, La Jolla, CA, 92037, USA*
[e] *College of Fisheries and Ocean Sciences, University of Alaska Fairbanks, Fairbanks, AK, 99775, USA*
[f] *Department of Biosciences, Rice University, Houston, TX, 77004, USA*

ARTICLE INFO

ABSTRACT

The eastern Indian Ocean is substantially under sampled with respect to the biological carbon pump – the suite of processes that transport the carbon fixed by phytoplankton into the deeper ocean. Using sediment traps and other ecosystem measurements, we quantified sinking organic matter flux and investigated the characteristics of sinking particles in waters overlying the Argo Abyssal Plain directly downstream of the Indonesian Throughflow off northwest Australia. Carbon export from the euphotic zone averaged 7.0 mmol C m^{-2} d^{-1}, which equated to an average export efficiency (export/net primary production) of 0.19. Sinking particle flux within the euphotic zone (beneath the mixed layer, but above the deep chlorophyll maximum) averaged slightly higher than flux at the base of the euphotic zone, suggesting that the deep euphotic zone was a depth stratum of net particle remineralization. Carbon flux attenuation continued into the twilight zone with a transfer efficiency (export at euphotic depth + 100m/export at euphotic depth) of 0.62 and an average Martin's *b*-value of 1.1. Within the euphotic zone, fresh phytoplankton (chlorophyll associated with sinking particles, possibly contained within appendicularian houses) were an important component of sinking particles, but beneath the euphotic zone the fecal pellets of herbivorous zooplankton (phaeopigments) were more important. Changes in carbon and nitrogen isotopic composition with depth further reflected remineralization processes occurring as particles sank. We show similarities with biological carbon pump functioning in a similar semi-enclosed oligotrophic marginal sea, the Gulf of Mexico, including net remineralization across the deep chlorophyll maximum.

1. Introduction

Net primary production (NPP) by phytoplankton decreases the partial pressure of CO_2 in the upper ocean, leading to CO_2 flux from the atmosphere into the oceans. However, most of the fixed carbon is rapidly consumed and recycled in the surface ocean with only a portion transported into the deeper ocean by a suite of processes referred to as the biological carbon pump (BCP) (Martin et al., 1987; Buesseler and Boyd, 2009; Boyd et al., 2019). Globally, the BCP is estimated to account for 5–13 Pg C yr^{-1} of flux into the deep ocean (Henson et al., 2011, 2022;

Laws et al., 2011; Siegel et al., 2014), although uncertainty is substantial and the BCP is highly variable at multiple spatial and temporal scales (Puigcorbé et al., 2017; Stukel et al., 2017; Smith et al., 2018).

The BCP includes multiple transport mechanisms, including active vertical migrations of zooplankton and nekton and passive transport of organic matter within subducted water (Carlson et al., 1994; Steinberg et al., 2000; Davison et al., 2013; Omand et al., 2015). However, the BCP is typically dominated by the carbon export of sinking particles (Nowicki et al., 2022; Stukel et al., 2022a, 2023) involving processes that package smaller cells into aggregates and fecal pellets that can sink at speeds of

---

hundreds of meters per day (Passow et al., 2001; McDonnell and Buesseler, 2010; Turner, 2015). The variety of ecological and biogeochemical processes involved, and their variability in time and space, complicate attempts to predict future changes in the BCP and marine carbon sequestration (Laufkötter et al., 2016; Henson et al., 2022).

Relative to the other major oceans, the Indian Ocean (IO) is substantially under sampled with respect to BCP-relevant processes (Hood et al., 2024a). It is a heterogeneous ocean with regions that are both net sources and net sinks for carbon dioxide (Bates et al., 2006; Ghosh et al., 2024; Hood et al., 2024b). The Arabian Sea, perhaps the most well-studied IO region, is strongly monsoon-influenced with high productivity during the southwest monsoon but with temporal variability at other scales and substantial spatial variability in productivity-limiting processes (Kumar et al., 2000; Barber et al., 2001; Marra and Barber, 2005). Substantial variability in sinking carbon export flux of this region follows from its diversity of productivity and trophic conditions (Buesseler et al., 1998; Lee et al., 1998; Honjo et al., 1999; Sarma et al., 2003; Rixen et al., 2019). A north-south transect from the Arabian Sea (17°N to 12°S) showed low export efficiency of 1.0–4.4 % of primary production leaving the euphotic zone during boreal spring, its most oligotrophic state (Subha Anand et al., 2018). In contrast, few carbon export measurements are available for the eastern IO, although the low export efficiency during oligotrophic conditions in the Arabian Sea is likely a reasonable expectation for similarly oligotrophic conditions in other IO regions.

This study focuses on export processes overlying the Argo Abyssal Plain, a deep oceanic basin (hereafter, Argo Basin) in the eastern Indian Ocean (Fig. 1) that was investigated as part of the Second International Indian Ocean Expedition (IIOE-2). The Argo Basin is bounded on the south by northwestern Australia and on the north by the Indonesian archipelago. Remote sensing products show that it is a tropical, oligotrophic system with low surface chlorophyll concentration and suggest low net primary production throughout the year (Kehinde et al., 2023; Hood et al., 2024b). The Argo Basin is the only known spawning site of Southern Bluefin tuna (Davis et al., 1990) and biogeochemically interesting as the terminus of the Indonesian Throughflow, the only low-latitude connection between the Pacific and Indian Oceans (Domingues et al., 2007; Sprintall et al., 2024). On the BLOOFINZ-IO (Bluefin Larvae in Oligotrophic Ocean Foodwebs, Investigations of Nutrients to Zooplankton – Indian Ocean, Landry et al. (this issue-a) Cruise in Jan–Mar 2021, we measured the magnitude and characteristics of sinking particles within and beneath the euphotic zone of the Argo Basin. We use these results to quantify and test the expected inefficiency of the BCP in this oligotrophic spawning region and to investigate its ecological controls. We also compare dynamics of the deep chlorophyll maximum of the Argo region to another oligotrophic bluefin tuna spawning basin in the deepwater Gulf of Mexico that has many similar characteristics as a warm, deep-water, oligotrophic region and was sampled by similar methods as part of the BLOOFINZ-GoM Program (Gerard et al., 2022).

2. Methods

2.1. Experimental design and water column measurements

Samples were collected in the Argo Basin in the eastern Indian Ocean as part of the BLOOFINZ-IO cruise from January–March 2022 (Landry et al. (this issue-a)). As with the companion study in the Gulf of Mexico (Knapp et al., 2021, Gerard et al., 2022), this cruise was organized around Lagrangian experiments (hereafter "cycles"). Water parcels of interest with respect to physical and biotic characteristics were identified through a combination of satellite imagery, ship underway flow-through data, and repeated net sampling (Landry et al. (this issue-a)). Water parcels were then followed using a pair of floating arrays. Both arrays included a satellite-enabled surface float tethered to a 3 × 1-m holey sock drogue (Landry et al., 2009). One array (described
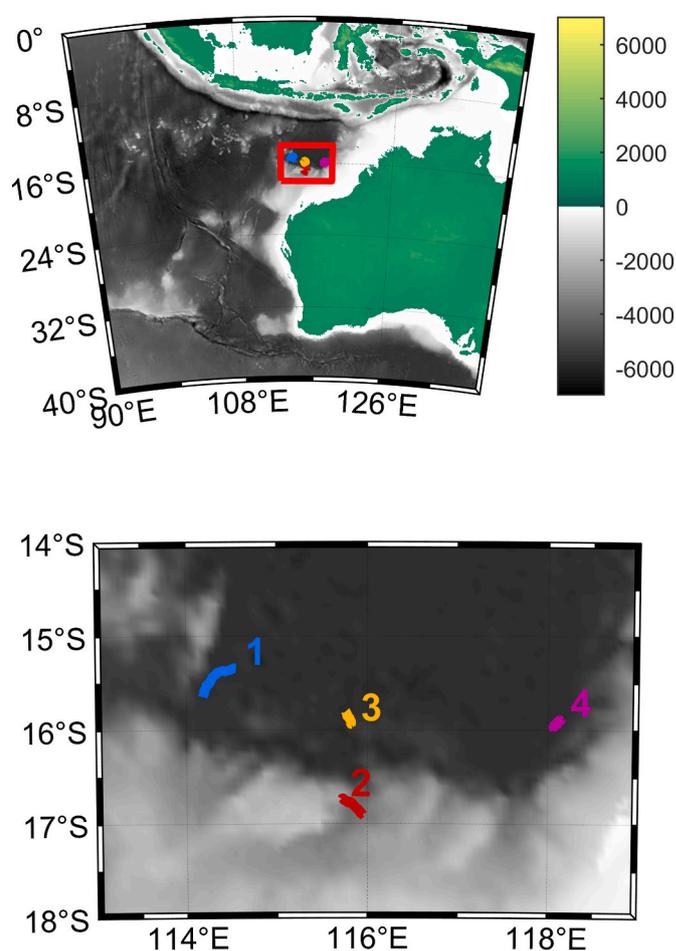

Fig. 1. Map of the study region with the top panel showing the broader area and bottom panel the study region itself, depicted with a red box on the top panel. Color represents elevation in both. Lagrangian trajectories of sediment traps are shown and labelled by cycle. (For interpretation of the references to colour in this figure legend, the reader is referred to the Web version of this article.)

further below) also included sediment trap crosspieces for collecting sinking particles. The other array ("incubation array") had stainless steel rings integrated into the line at fixed depths below the surface float for attaching mesh bags containing experimental bottles that were incubated in situ for 24-hr periods to measure net primary production and other ecosystem rates (Landry et al., 2009).

Lagrangian experiments lasted from 3.3 to 4.3 days. At 02:00 local time each day, a CTD with attached Niskin rosette was deployed to measure vertical profiles of temperature, salinity, fluorescence, and oxygen and to collect samples from 6 depths (from the near surface to the DCM depth) for nutrients, chlorophyll *a* (Chl*a*), particulate organic matter (POM), and NPP measurements. Chl*a* and POM were also measured at additional deeper depths. Nutrient samples were filtered through a 0.1-μm Acropak cartridge filter and stored frozen until analysis for nitrate + nitrite, nitrite, ammonium, phosphate, and silicic acid using an autoanalyzer at the Scripps Institution of Oceanography, Ocean Data Facility. Samples for Chl*a* and phaeopigments were filtered through glass fiber fine (GF/F) filters at low vacuum pressure and measured on a Turner 10AU fluorometer using the acidification method after 24-h acetone extraction at −20 °C. POM samples (4-L) were filtered through pre-combusted GF/F filters, which were dried until analysis on land. Filters were then acidified to remove inorganic carbon, packed into pre-combusted tin capsules and analyzed for carbon, nitrogen, and isotopes at the University of California, Davis, Stable Isotope Facility.

Phytoplankton community composition was quantified using a

combination of flow cytometry for picoplankton (<2 μm) and epifluorescence microscopy for nano- and microplankton (Yingling et al). Samples for phytoplankton community composition were collected daily from the same depths as chlorophyll, nutrients, and net primary production. Picophytoplankton biomass was estimated from FCM abundances assuming a cellular carbon content of 36, 101 and 359 fg C cell^{-1} for *Prochlorococcus*, *Synechococcus*, and picoeukaryotes, respectively (Yingling et al). The biomass of nano- and microphytoplankton was estimated using biovolume measurements from epifluorescence microscopy and allometric carbon:volume relationships from Menden-Deuer and Lessard (2000).

Triplicate samples (plus a dark blank) for net primary production were gently transferred to polycarbonate bottles which were spiked with H^{14}CO$_3^-$ and incubated at in situ depths on the incubation array for 24 h. After recovery, samples were filtered through GF/F filters and ^{14}C radioactivity was determined with a liquid scintillation counter (Kranz et al., 2026). An Underwater Vision Profiler 6 (UVP6) was attached to the CTD-Niskin rosette and used to measure vertical profiles of the particle volume-size spectrum (Picheral et al., 2022). We restricted analysis of this data to particles (including aggregates) with sizes ranging from 51 to 1290 μm. Below 51 μm, pixel-level noise made the data untrustworthy; above 1290 μm the sampled volume was too low for reasonable particle count estimates.

2.2. Sediment traps

VERTEX-style sediment trap crosspieces (Knauer et al., 1979) were attached to the sediment trap array at four depths: beneath the mixed layer (52–62 m), near the base of the euphotic zone as estimated from fluorescence profiles (116–127 m), and in the mesopelagic zone at ~220 and ~420 m depth. Aqualogger pressure-temperature sensors were used to measure actual depths of trap deployments. Twelve particle interceptor tubes (7-cm inner diameter, 8:1 aspect ratio, topped with a baffle constructed of 14 smaller tubes that were tapered on the top) were attached to each crosspiece at the three shallowest depths (16 tubes at the deepest depth). Tubes were deployed with a seawater brine made from 0.1-μm seawater amended with 50 g L^{-1} NaCl and formaldehyde (0.4 %, final concentration) and left for 3.3–4.3 days. After recovery, overlying water was immediately removed from each tube by gentle suction. Samples were then filtered through a 100-μm Nitex filter and the filter was inspected at 25X magnification under a stereomicroscope to remove zooplankton "swimmers". Contents of filters (i.e., non-swimmer sample) were then washed back into the filtrate ($<$100-μm portion of the sample). Three tubes per depth were filtered through pre-combusted GF/F filters for carbon, nitrogen, and isotope samples (analyzed as described above), and 50-mL subsamples were taken from three separate tubes and analyzed for Chl*a* and phaeopigments as described above. To interpolate flux measurements to exactly the base of the euphotic zone (which we define as the 0.1 % light level) and to a depth 100 m greater than the euphotic depth, we use a power law fit (Supp. Table 1).

2.3. BLOOFINZ-GoM comparison cruise

Nearly identical experimental methods were used as part of the BLOOFINZ-GoM companion cruises in an oligotrophic area of the Gulf of Mexico (Gerard et al., 2022; Stukel et al., 2022b). This region is similar to the Argo Basin as a semi-enclosed basin with a deepwater, oligotrophic interior that is a primary spawning site for bluefin tuna larvae (Southern Bluefin tuna in Argo Basin, Atlantic Bluefin tuna in Gulf of Mexico). BLOOFINZ-GoM cruises were conducted in May 2017 (BLOOFINZ-GoM Cycles 1–3) and May 2018 (BLOOFINZ-GoM Cycles 4–5). Slight methodological differences between cruises include the absence of a deep ($>$400 m) sediment trap cross-piece (Stukel et al., 2021), the use of H^{13}CO$_3^-$ instead of H^{14}CO$_3^-$ to measure NPP (Yingling et al., 2022), and lack of a UVP6 in the GoM.

3. Results

3.1. Oceanographic and water column conditions in the Argo Basin

The surface ocean was warm and strongly stratified throughout the cruise. The deepest cycle-average mixed layer depth (defined as a 0.01 kg m^{-3} increase in potential density relative to the average potential density of the upper 5 m) was 30.5 m for Cycle 1, which was conducted shortly after a storm moved through the region. Even for this cycle, however, surface temperatures exceeded 28 °C (Fig. 2a). For the other cycles, cycle-average mixed layer depth was always shallower than 10 m (Fig. 2b), while sea surface temperatures (calculated at 5-m depth) were 28.8, 29.8, and 30.5 °C for Cycles 2–4, respectively.

Warm surface temperatures and stratified conditions were paired with strong deep chlorophyll maxima (DCM) that ranged from 67 (Cycle 3) to 75 m (Cycle 1) depth (Fig. 2d and 3a). Chl*a* concentrations were much higher at the DCM (cycle averages ranged from 0.29 to 0.56 mg Chl*a* m^{-3}) than at the surface (0.07–0.09 mg Chl*a* m^{-3}). Nitrate concentration was consistently low above 50 m with an average of 0.016 μmol L^{-1} across all samples and a maximum measured value (above 50 m) of 0.12 μmol L^{-1}. Nitracline depths (defined as the depth at which nitrate first exceeded 1 μmol L^{-1}) were near the DCM, with cycle-average nitracline depths ranging from 66 to 78 m. The cycle-average depths of the euphotic zone (here, defined as the depth of the 0.1 % light level) ranged from 121 to 127 m. Oxygen concentrations were near saturation with the atmosphere in the upper ~50 m, but decreased rapidly with depth beneath 50 m and typically were ~50 % saturation at ~200-m depth (Fig. 2c). In contrast to chlorophyll, particulate organic carbon (POC) concentrations varied only weakly with depth in the upper 250 m of the water column. POC increased slightly with depth from the surface to the DCM and then decreased mostly monotonically with depth in deeper waters. Despite these trends, POC typically varied within a small range of 2–5 mmol C m^{-3} throughout the epipelagic (Fig. 3b). At most depths, Cycle 4 had lower Chl*a* and POC concentrations than the other cycles, although differences were relatively small. These slight differences may reflect temporal variation across the system as nutrients injected by the storm in the beginning of the cruise were consumed over the following weeks.

Using a UVP6, we obtained estimates of particle abundances and volumes (including aggregates and living organisms) as a function of particle diameter and depth (Fig. 4). Large particles and aggregates (100–1000 μm diameter) were typically most abundant in the DCM depth range. Large particles were also abundant in the shallowest depth stratum (0–5 m), although it is likely that images in this depth range were affected by bubbles forming near the ocean surface. Subsurface large particle maxima were most pronounced during Cycles 2 and 3. During Cycle 1, total particle volume only increased ~2-fold from the surface to the depth of the DCM, and large particle abundance integrated over the euphotic zone was substantially lower than on the other cycles. During Cycle 4, large particles had similar abundance at the deep chlorophyll maximum to Cycles 2 and 3, but large particle abundance was substantially greater in the depth range of ~20–50 m during Cycle 4, relative to other cycles. This increased abundance of large particles during the later portions of the cruise may reflect an increased abundance of appendicularians (filter-feeding pelagic tunicates that produce large mucous feeding mesh "houses"), which were found to increase in abundance by more than a factor of 2 during the cruise (Swalethorp et al). Beneath the DCM, large particle abundance decreased rapidly with depth for all cycles.

Vertically integrated NPP measured by H^{14}CO$_3^-$ uptake was relatively low, as expected, for oligotrophic waters, with an average across all profiles of 37 ± 3 mmol C m^{-2} d^{-1} (Supp. Table 1). NPP was substantially lower on Cycle 1 (21.8 ± 5.5 mmol C m^{-2} d^{-1}) than the other cycles (44.0 ± 3.8, 45.3 ± 4.1, and 41.0 ± 2.3 mmol C m^{-2} d^{-1}, for Cycles 2–4, respectively). Low NPP on Cycle 1 may have been tied to light limitation; Cycle 1 had the lowest average surface
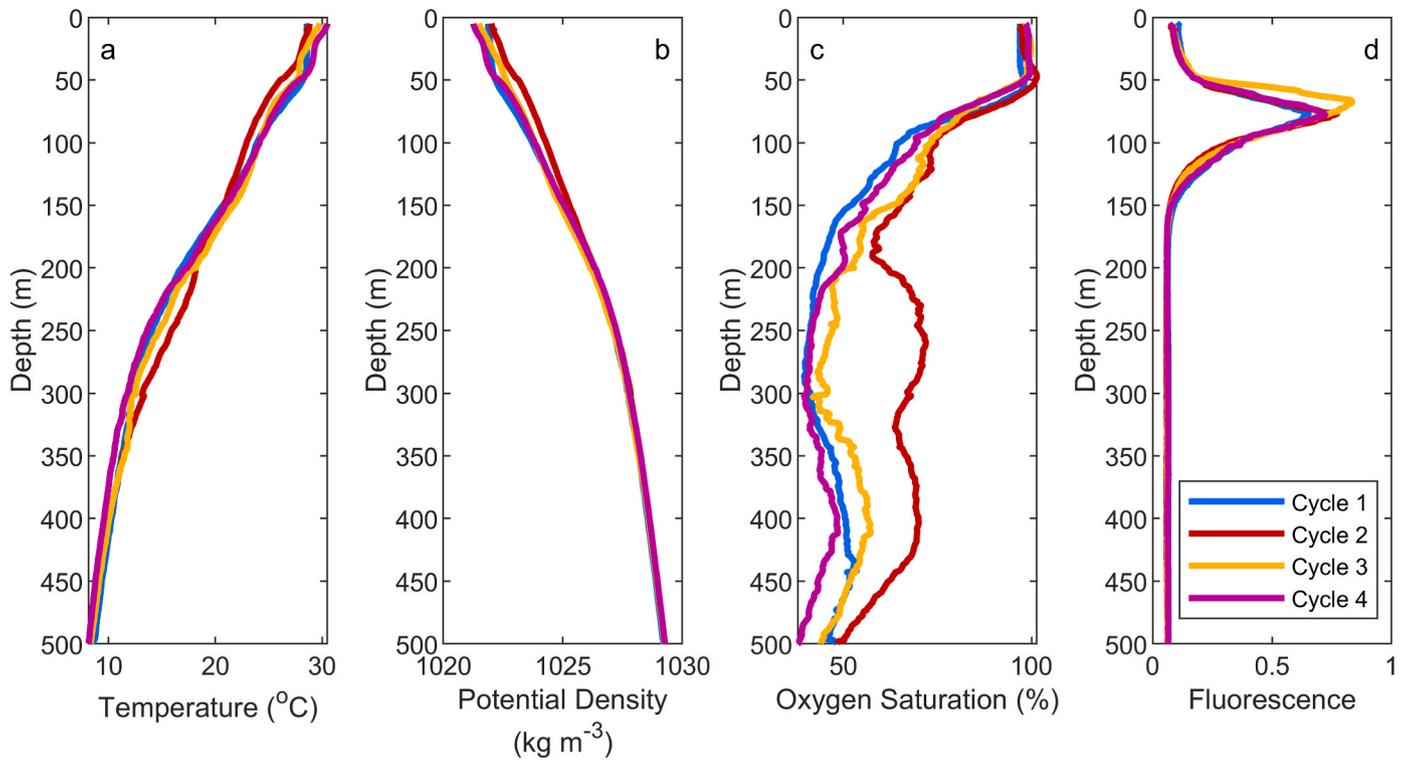
Fig. 2. Cycle average vertical profiles of (a) temperature, (b) potential density, (c) oxygen saturation, and (d) fluorescence (proxy for chlorophyll).
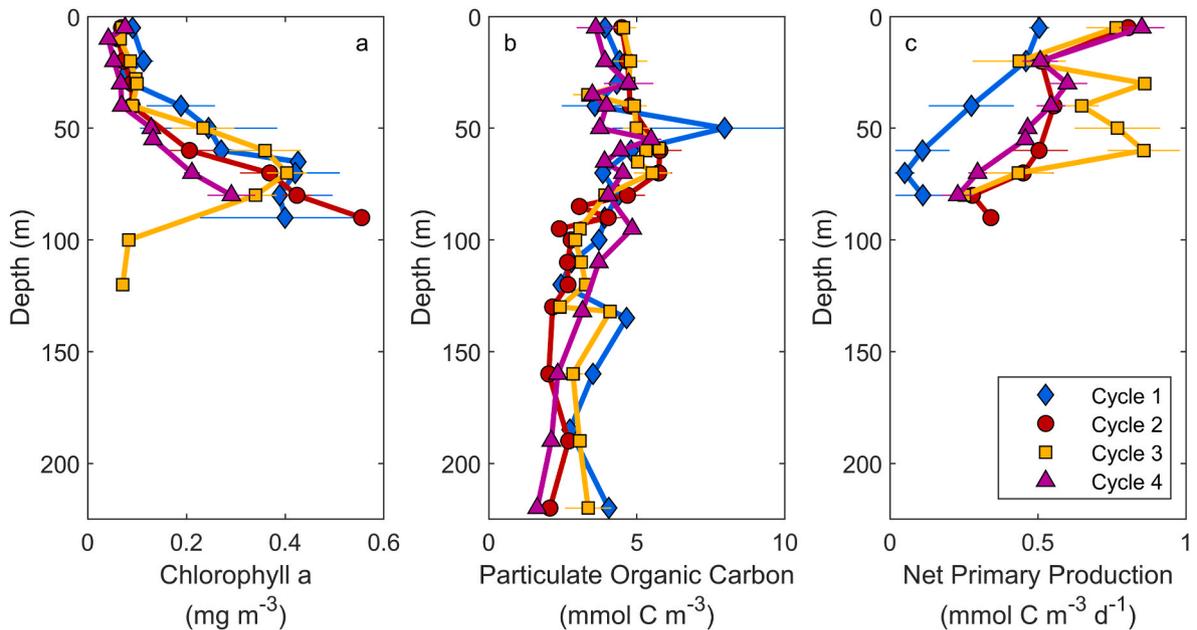

Fig. 3. Vertical profiles of (a) Chlorophyll *a*, (b) Particulate Organic Carbon, (c) Net Primary Production. Average values and standard error for each Lagrangian cycle are shown.

photosynthetically-active radiation. NPP generally decreased monotonically with depth, although Cycle 3 exhibited little change with depth in the upper 60 m. Despite strong chlorophyll maxima at 67–75 m depth, NPP was typically much lower at the DCM than in the mixed layer.

3.2. Sinking particle flux in the Argo Basin

Organic carbon fluxes into sediment traps near the base of the euphotic zone (trap depth of 116–127 m) averaged 7.3 mmol C m^{-2} d^{-1}

and ranged from 3.7 to 10.4 mmol C m^{-2} d^{-1} (Fig. 5a). Carbon fluxes during Cycles 1 and 2 were substantially lower than for Cycles 3 and 4. For traps placed at 52–62 m depth, below the mixed layer but above the DCM, carbon flux was actually higher on average (although not statistically different) than beneath the euphotic zone (mean = 8.1, range = 7.0–9.4 mmol C m^{-2} d^{-1}). On Cycles 1 and 2, organic carbon flux decreased across the DCM, while on Cycles 3 and 4 organic carbon flux increased across the DCM. Beneath the euphotic zone, carbon flux decreased monotonically with depth, averaging 3.9 mmol C m^{-2} d^{-1} at
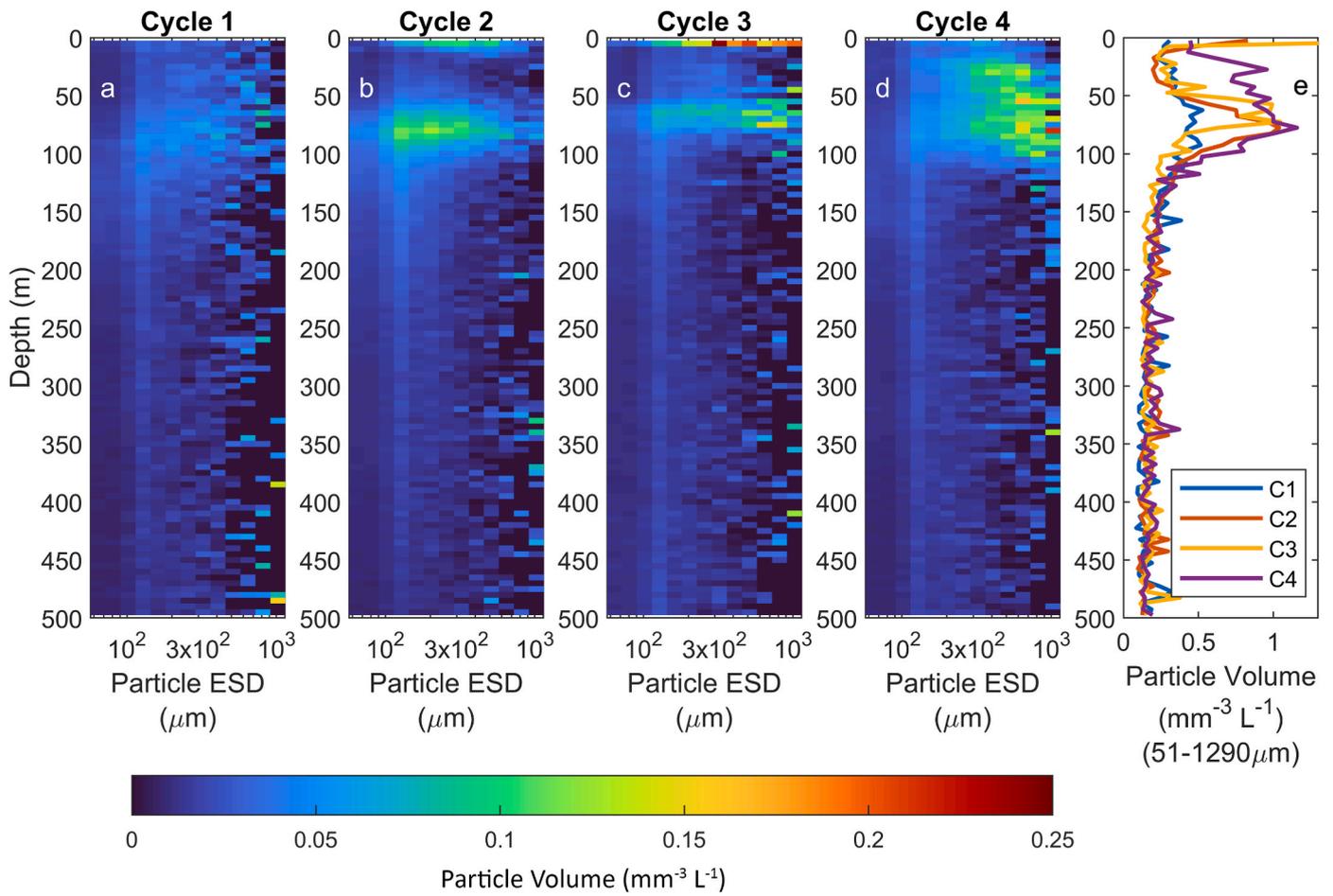
Fig. 4. Large particle volume estimated with the Underwater Vision Profiler 6 (UVP6) as functions of equivalent spherical diameter (ESD, x-axis in panels a–d) and depth. a – d represent mean particle volumes (mm^{-3} L^{-1}) from CTD casts for Cycles 1–4, respectively. Panel e shows summed particle volume across all size classes (from 51 to 1290 μm).
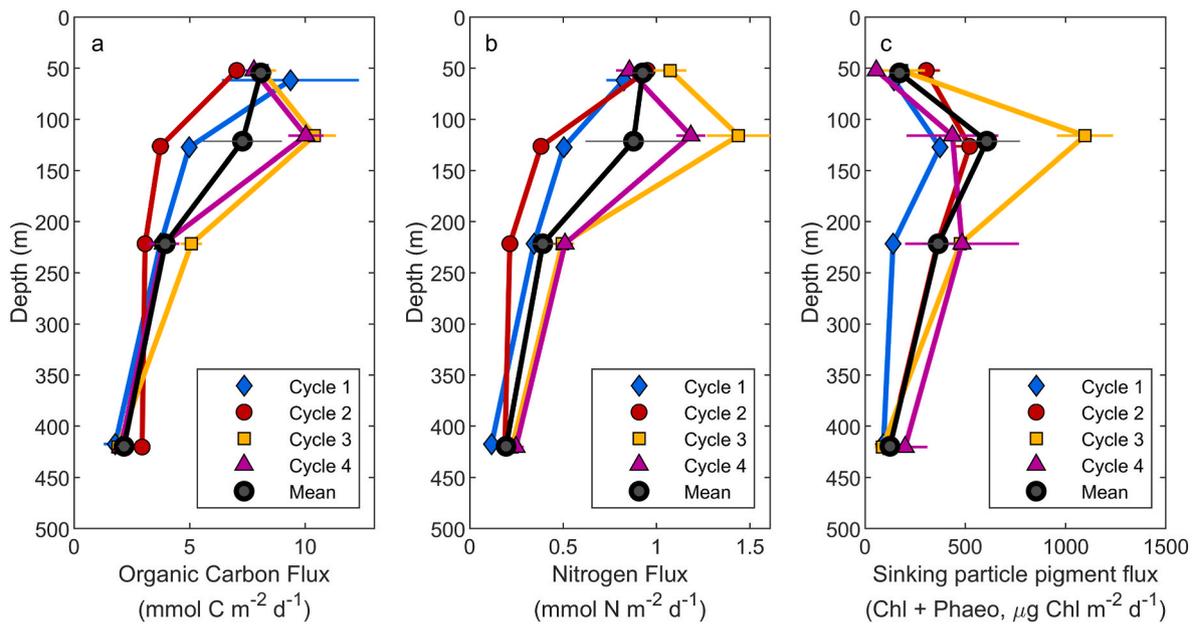

Fig. 5. Sinking particle fluxes measured by sediment traps. (a) Organic Carbon Flux. (b) Nitrogen Flux. (c) Pigment Plux (sum of chlorophyll *a* and phaeopigments). Error bars are ±1 standard error of the mean.

220 m (range 3.1–5.1 mmol C m^{-2} d^{-1}) and 2.2 mmol C m^{-2} d^{-1} at 420   m (range 1.8–2.9 mmol C m^{-2} d^{-1}). Combining data from all cycles, and

using the 0.1 % light level as the reference depth, a power law fit suggests an average Martin's b-value of 1.1. This is fairly typical of global ocean b-value estimates (Marsay et al., 2015), suggesting moderate flux attenuation with depth, but notably lower than expected for a warm-water region (typical b of 1.2–1.6, Lamborg et al., 2008; Marsay et al., 2015). Sinking nitrogen fluxes mostly mirrored the patterns in sinking carbon (Fig. 5b). For Cycles 3 and 4, the C:N ratios of sinking particles remained relatively constant with depth (ranging from 7.2 to 10.3 mol:mol), while for Cycles 1 and 2 the C:N ratio increased with depth to an average of 15.5 (mol:mol) at 420 m (Fig. 6a).

Carbon isotope values of sinking particles were lighter with depth, reflecting remineralization processes (Fig. 6b). This trend was consistent for all cycles and across all depths, except for an isotopically lighter sample at 200 m than at 420 m for Cycle 3. In comparison, nitrogen isotopes did not exhibit clear trends with depth. Nitrogen isotopes became isotopically heavier with depth for three cycles but showed no change or a slight decrease for Cycle 4, which was also isotopically lighter than the other cycles at shallow depths (Fig. 6c). Notably, suspended POM for Cycle 4 did not have similarly low $\delta^{15}N$ as the sinking particles, with Cycle 2 having the lowest $\delta^{15}N$ POM (Supp. Fig. 1). Looking across all samples, there was a strong inverse correlation between the $\delta^{13}C$ and $\delta^{15}N$ of sinking particles (Pearson's $\rho = -0.79$, p = 2.8×10^{-4}), but no similar correlation was found for suspended POM.

Total pigment (Chl$a$ + phaeopigment) flux on sinking particles increased substantially from above the DCM (average of 172 μg pigment m^{-2} d^{-1}) to beneath it (average of 607 μg pigment m^{-2} d^{-1}, Fig. 5c). This increase in pigment flux was associated with a shift from a substantial flux of Chl$a$ to predominantly phaeopigment flux. For Cycles
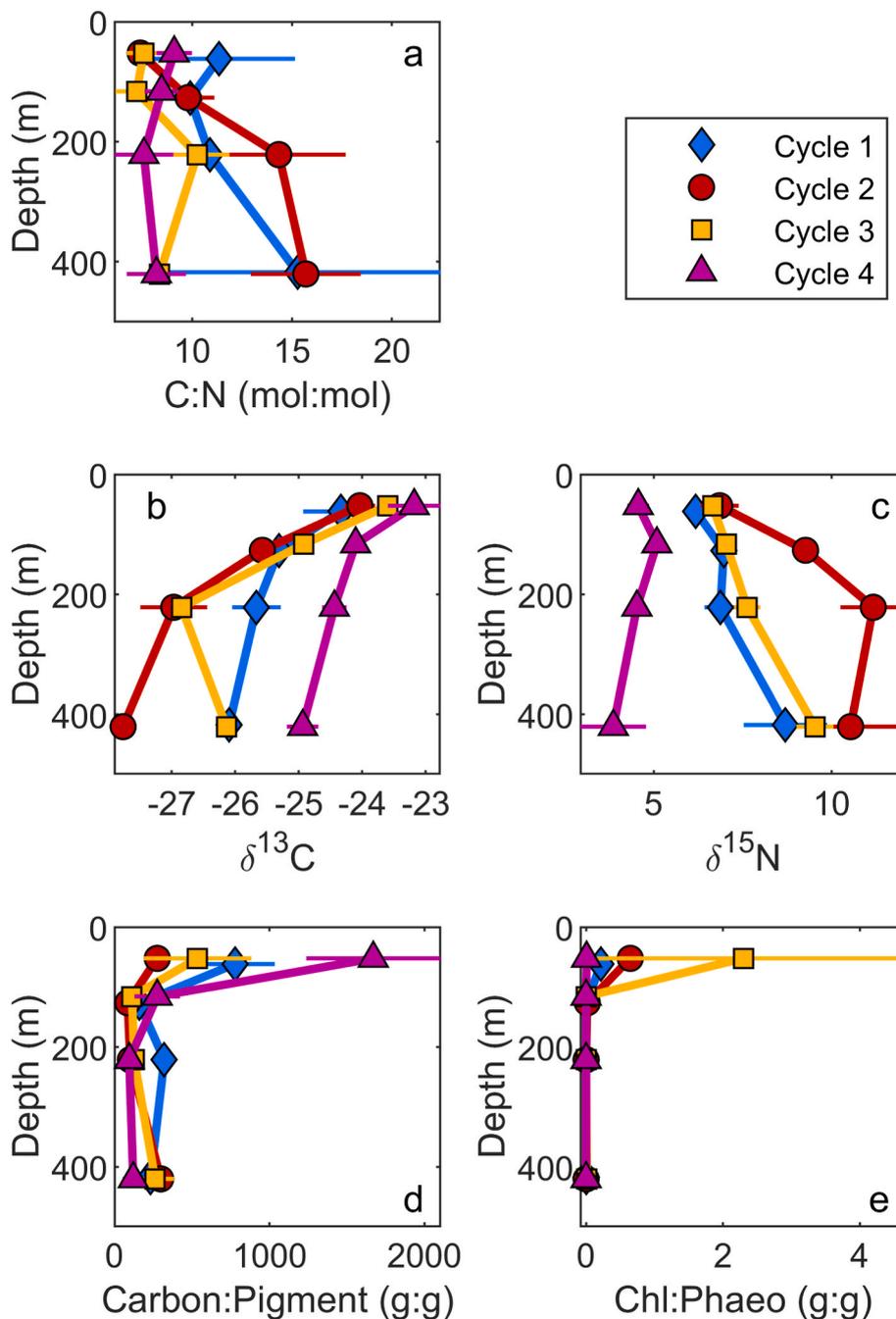

Fig. 6. Characteristics of sinking particles. a) Organic Carbon:Nitrogen Ratio, b) ^{13}Carbon Isotopic Values, c) ^{15}Nitrogen Isotopic Values, d) Carbon:Pigment Ratio (pigment = chlorophyll a + phaeopigments), e) Chlorophyll a:Phaeopigment Ratio. Means ± 1 standard errors are shown.

1–3, Chl*a* flux at 52–62 m ranged from 26 to 127 µg Chl*a* m^{-2} d^{-1} (mean of 90.8 µg Chl*a* m^{-2} d^{-1}). Beneath the euphotic zone (116–127 m), Chl*a* flux declined to 8.5 µg Chl*a* m^{-2} d^{-1} on Cycle 2 and was unmeasurable on all other cycles. In contrast, phaeopigment flux at 116–127 m increased to 374–1097 µg Chl*a* m^{-2} d^{-1}. Because phaeopigments are generally indicative of fecal pellets produced by herbivorous zooplankton, this suggests a shift from sinking of uningested phytoplankton within the euphotic zone to primarily sinking fecal pellets exiting the euphotic zone. Phaeopigment flux then declined gradually with depth beneath the euphotic zone, with carbon:pigment ratios of sinking particles remaining relatively constant with depth (Fig. 6d). The decrease in carbon:total pigment flux within the euphotic zone likely reflects a change in the carbon:Chl*a* ratio of phytoplankton with depth. Based on flow cytometry and epifluorescence microscopy-based estimates of phytoplankton carbon biomass (Yingling et al), phytoplankton carbon:Chl*a* ratios averaged 130 g:g in the upper 50 m of the water column, and decreased to an average of 37 g:g in the 70–100 m depth range. If we assume that 130 g:g is representative of phytoplankton sinking into our shallowest sediment trap, then sinking phytoplankton flux ranged from 0.004 to 1.4 mmol C m^{-2} d^{-1} (with a mean of 0.74 mmol C m^{-2} d^{-1}) and contributed up to 18 % of sinking carbon above the DCM. These undigested sinking phytoplankton may have been attached to discarded appendicularian houses. These houses can be efficient mechanisms for concentrating small phytoplankton carbon into larger particles capable of relatively fast settling rates (Alldredge, 2005; Lombard and Kiorboe, 2010).

Beneath the euphotic zone, sinking carbon flux of uneaten phytoplankton was negligible. However, if we take 37 g:g as an estimate of the carbon:Chl*a* of phytoplankton consumed by herbivorous zooplankton in the deep euphotic zone and that 70 % of the ingested carbon is consumed while all of the chl*a* is converted to phaeopigments, then herbivore fecal pellets were responsible for 3.8–11.2 mmol C m^{-2} d^{-1} (with a mean of 6.2 mmol C m^{-2} d^{-1}) and contributed to 45–141 % of sinking carbon.

4. Discussion

4.1. The biological carbon pump in the Argo Basin and Gulf of Mexico

The oligotrophic central waters of the Gulf of Mexico is an interesting site for comparison with the Argo Basin, because it is also a semi-enclosed, tropical, deep-water basin and crucial spawning site for bluefin tuna (Atlantic Bluefin in the Gulf of Mexico, Southern Bluefin in the Argo Basin). Conditions encountered during the BLOOFINZ-GoM study were even more oligotrophic than those during the BLOOFINZ-IO cruise (Gerard et al., 2022). Nitracline and DCM depths during BLOOFINZ-GoM were deeper than in the Argo Basin (84–127 m and 78–137 m, respectively, in the GoM, Knapp et al., 2021; Landry et al., 2021, compared to 66–78 m and 67–75 m, respectively in the Argo Basin). Surface Chl*a* was similar to BLOOFINZ-IO (0.05–0.13 mg m^{-3}) and *Prochlorococcus* dominated phytoplankton community biomass in both regions (Selph et al., 2021; Yingling et al). Sea surface temperatures were substantially cooler (~26 °C) in the Gulf of Mexico than in the present study (28.8–30.5 °C).

Across the five BLOOFINZ-GoM cycles, NPP ranged from 24.3 to 29.3 mmol C m^{-2} d^{-1}, which was lower than all but Cycle 1 of BLOOFINZ-IO (Fig. 7a). At other well-studied oligotrophic regions NPP typically averages ~38 mmol C m^{-2} d^{-1}; the range at the Hawaii Ocean Timeseries site in the North Pacific Subtropical Gyre is 26–49 mmol C m^{-2} d^{-1} and the range at the Bermuda Atlantic Time-Series site in the Sargasso Sea is 27–44 mmol C m^{-2} d^{-1} (Church et al., 2013). The Argo Basin thus exhibited fairly typical NPP during our cruise, while the Gulf of Mexico had slightly below average NPP, reflecting its extremely low levels of nutrients in the upper 100 m and very deep chlorophyll maxima. In contrast to those other oligotrophic sites, however, the Argo Basin and Gulf of Mexico had relatively high export efficiency. The EZ-ratio (ratio of export at the base of the euphotic zone to NPP) ranged from 0.085 to 0.23 for BLOOFINZ-IO and from 0.11 to 0.25 for BLOOFINZ-GoM (Fig. 7b). These EZ-ratios, averaging 0.19 for
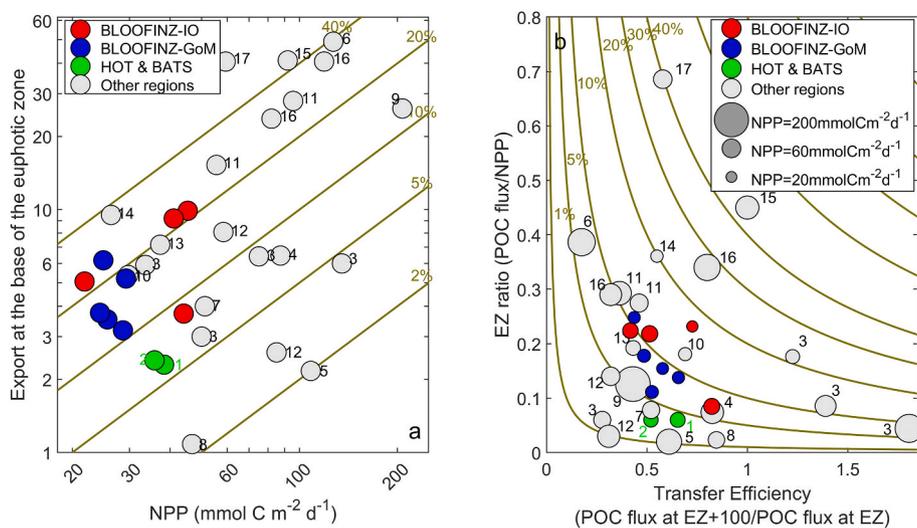

Fig. 7. Comparisons of BLOOFINZ export to other regions. (a) shows sinking organic carbon flux at the base of the euphotic zone (0.1 % light level) as a function of net primary production (NPP), with gold lines showing isopleths of constant EZ-ratio. (b) shows EZ-ratio plotted against transfer efficiency (T$_{100}$ = export flux at euphotic depth + 100 m/export flux at euphotic depth). Gold lines show isopleths of constant percentage of NPP exported 100 m deeper than euphotic depth. In both panels red symbols are from Argo Basin (see Supp. Table 1 for data), blue symbols are from Gulf of Mexico, and green symbols are from mean values from the warm-water, oligotrophic Hawaii Ocean Time-series (North Pacific Subtropical Gyre, [1](Church et al., 2013)) and Bermuda Atlantic Time-Series (Sargasso Sea, [2](Lomas et al., 2013)) Programs. With the exception of BLOOFINZ symbols, all results are means from multiple sediment trap deployments or [234]Th profiles in a specific region. [3]Sargasso Sea eddies (Buesseler et al., 2008a). [4]Costa Rica Dome (Stukel et al., 2016). [5]Equatorial Pacific (Bacon et al., 1996). [6]Tropical South Pacific, shelf (Black et al., 2018). [7]Tropical South Pacific, offshore (Black et al., 2018). [8]Tropical South Pacific, gyre (Black et al., 2018). [9]California Current Ecosystem, coastal upwelling (Stukel and Barbeau, 2020). [10]California Current Ecosystem, offshore oligotrophic (Stukel and Barbeau, 2020). [11]California Current Ecosystem, frontal regions (Krause et al., 2015; Stukel et al., 2017). [12]Subarctic Pacific (Charette et al., 1999). [13]Subarctic Pacific (Buesseler et al., 2008b). [14]Spanish continental margin (Olli et al., 2001). [15]North Atlantic Bloom (Buesseler et al., 1992). [16]Southern Ocean (Buesseler et al., 2003). [17]Barents Sea (Andreassen and Wassmann, 1998). (For interpretation of the references to colour in this figure legend, the reader is referred to the Web version of this article.)

BLOOFINZ-IO and 0.17 for BLOOFINZ-GoM, are substantially higher than typically expected for oligotrophic systems dominated by small phytoplankton (usually <10 %, with a typical value of 5 %, Buesseler and Boyd, 2009; Siegel et al., 2014; Karl et al., 2021; Stukel et al., 2024). Export is expected to be inefficient in these systems for multiple reasons: The supply of new nutrients necessary to support export (new production) is low (Eppley and Peterson, 1979; Harrison et al., 1987); the picoplankton that dominate the system are too small to sink individually (Smayda, 1970); and food-web pathways that convert phytoplankton into rapidly sinking zooplankton fecal pellets are typically long and inefficient (Michaels and Silver, 1988; Steinberg and Landry, 2017). These criteria for low export efficiency are all met in both regions: nutrient concentrations are too low to suggest substantial upwelled nitrate; *Prochlorococcus* dominates the phytoplankton biomass (Selph et al., 2021; Yingling et al); and food chains are long with substantial energy dissipation through the microbial loop (Landry et al., 2021; Stukel et al., 2022b; Stukel et al., this). High export efficiency is thus surprising, although it may be related to lateral transport from the adjacent productive coastal areas. Kelly et al. (2021) showed that all of the measured export flux for BLOOFINZ-GoM could be supported by lateral transport of POM (both living and dead) from the shelf region. Similarly, Kehinde et al. (2023) suggested that 32 % (but with an uncertainty range of 10 - >100 %) of export during BLOOFINZ-IO could be supported by lateral transport of POM. It is possible that this POM subsidy is additive to the normal low export efficiency of oligotrophic systems, although it is important to note that at the warm temperatures in the region, we should expect particles to be consumed, re-worked and/or recycled multiple times in the euphotic zone before sinking. Additionally, it is likely that the typical relationship between phytoplankton size and export efficiency was substantially modified by the observed importance of appendicularians (Swalethorp et al), which feed efficiently on picoplankton and produce large marine snow aggregates through their discarded mucus houses (Alldredge, 2005).

Particle transfer efficiency through the shallow twilight zone was moderate. The ratio of export at a depth horizon 100 m beneath the euphotic depth (0.1 % light level) divided by export at the euphotic depth (T_{100} = flux transfer efficiency over 100 m) averaged 0.62 during BLOOFINZ-IO and 0.54 during BLOOFINZ-GoM (Fig. 7b–Supp. Table 1). T_{100} was notably higher for Cycles 1 and 2 of BLOOFINZ-IO (0.73 and 0.82) than for Cycles 3 and 4 (0.51 and 0.42). These differences were driven by greater variability in export flux at the base of the euphotic zone than at other depths (Fig. 5a). The coefficient of variation (standard deviation/mean) for export flux interpolated to the base of the euphotic zone was 0.44, while the coefficient of variation was only 0.21 at a depth of ~220 m and 0.25 at a depth of ~420 m. Decreased variability in export flux in the mesopelagic relative to the base of the euphotic zone is likely a result of the "statistical funnel" effect (Siegel et al., 2008); with increasing depth in the ocean the area of surface productivity that contributes to export measured at a specific location increases as a result of the lag time introduced by slow and variable particle settling speeds and rapid horizontal currents. This spatiotemporal averaging dampens the variability that exists in surface production.

Decreasing organic matter flux with depth was also associated with substantial shifts in the isotopic composition of sinking material. In both the GoM and Argo Basin, $\delta^{15}N$ values generally increased with depth and $\delta^{13}C$ values generally decreased with depth (Fig. 6 and Stukel et al., 2021). While the distinctly low $\delta^{15}N$ for BLOOFINZ-IO Cycle 4 is likely indicative of recent diazotrophy (Kranz et al., 2026), the strong correlation between $\delta^{15}N$ and $\delta^{13}C$ (Supp. Fig. 1f) suggests that remineralization processes may broadly drive patterns in both of these isotopes. Higher $\delta^{15}N$ of sinking particles at deeper depths likely reflects isotopic fractionation as many metabolic processes preferentially utilize ^{14}N (Post, 2002; Glibert et al., 2019). Conversely, lower $\delta^{13}C$ suggests preferential utilization of organic compounds with comparatively high $\delta^{13}C$; more specifically, lipids have low $\delta^{13}C$ and typically remain within sinking particles after amino acids have been remineralized

(McConnaughey and McRoy, 1979; Wakeham and Lee, 2019).

During both BLOOFINZ-GoM and -IO studies, we deployed sediment traps in the euphotic zone at a depth of ~50–60 m, beneath the mixed layer but above the DCM. Both studies showed that sinking carbon flux attenuation began within the euphotic zone. Organic carbon flux decreased from a mean of 8.1 mmol C m^{-2} d^{-1} at the shallowest depth to a mean of 7.0 mmol C m^{-2} d^{-1} at the base of the euphotic zone (0.1 % light level) during BLOOFINZ-IO. It decreased even more strongly across this depth horizon during BLOOFINZ-GoM, declining from 6.4 to 4.4 mmol C m^{-2} d^{-1} (Supp. Fig. 2). This pattern of decreasing export flux through the deep euphotic zone was also more consistent in the Gulf of Mexico, declining during four out of five Lagrangian cycles. These changes in export flux with depth also included an increase in the pigment:carbon ratio and decrease in the Chl*a*:phaeopigment ratio for sinking particles in both BLOOFINZ-IO and BLOOFINZ-GoM, suggesting a switch from sinking phytoplankton within the euphotic zone to sinking fecal pellets at the base of the euphotic zone.

Particle size spectra can also be used to investigate processes relating to particle export and how it varies with depth. While early studies suggested that the particle (and aggregate) size spectra generated by the UVP could estimate sinking particle fluxes optically (Guidi et al., 2008), subsequent studies have shown that any such algorithms need to be regionally tuned (Iversen et al., 2010; Fender et al., 2019) and are likely not constant with depth (Fender et al., 2019). The variability in particle size-flux algorithms argues against treating UVP data as a reliable estimator of the absolute magnitude of sinking carbon flux. Nevertheless, comparison of sediment trap rates to UVP estimates of export flux from previously published algorithms allows us to investigate how the particle size – sinking speed relationship may change with depth (Supp. Fig. 3). Although none of the three algorithms provided accurate estimates of export, all showed similar patterns. Specifically, samples collected in the shallowest sediment traps had consistently lower particle fluxes than predicted by the algorithms, while the greatest underestimate by the UVP algorithms was for sediment traps located immediately beneath the euphotic zone (specifically on Cycles 3 and 4). This would suggest that particles and aggregates of a specific size were sinking more slowly within the euphotic zone (where high Chl*a*:C ratios indicated sinking phytoplankton that were loosely associated with aggregates or appendicularian houses) and more rapidly immediately beneath the euphotic zone (where high phaeopigment:C ratios indicated sinking fecal pellets).

Zooplankton also contribute to carbon export by feeding in the surface ocean during the night and descending to mesopelagic depths during the day where their respiration leads to a net downward carbon transport (Longhurst et al., 1990; Steinberg et al., 2000). (Décima et al) (this issue) measured day-night differences in zooplankton biomass and applied allometric scaling equations to estimate diel-vertical-migrating zooplankton respiration in the mesopelagic zone. They calculated active transport rates ranging from 0.42 to 0.70 mmol C m^{-2} d^{-1}, which equates to only 4–14 % of the sinking carbon export that we measured at the base of the euphotic zone. However, as most of these vertical migrants likely migrate to depths >400 m during the day, this may be equal to 18–35 % of the sinking carbon that reached our deep sediment traps at ~420 m. For the GoM, Kelly et al. (2021) estimated that active transport was equal to a similar ~10 % of sinking particle export flux at the base of the euphotic zone. These modest estimates of active transport are similar to those found in other oligotrophic regions. For instance, at the Hawaii Ocean Time-series site, vertical migrants were responsible for 19 % of the carbon exported as sinking particles (Hannides et al., 2009), while at the Bermuda Atlantic Time-series site they were responsible for 8 % (Steinberg et al., 2000). These results point to an emerging view that active transport is a minor, but not negligible component of export flux in low-productivity regions (Archibald et al., 2019; Nowicki et al., 2022; Stukel et al., 2022a), although the deep depth of respiratory C loss for vertical migrants can lead to disproportionately high carbon sequestration (Bianchi et al., 2013; Boyd et al.,

2019; Stukel et al., 2023).

4.2. Particle flux and the functioning of the deep chlorophyll maximum

Sediment traps are seldom deployed in the euphotic zone. One reason for this is that hydrodynamic biases can be especially pronounced during turbulent conditions in the mixed layer (Baker et al., 1988; Buesseler et al., 2007). This issue is unlikely to be problematic, however, in strongly stratified conditions with shallow mixed layers as encountered on the BLOOFINZ-GoM and BLOOFINZ-IO cruises, and indeed in many areas with prominent DCMs. Another reason that sediment traps are usually only deployed beneath the euphotic zone is that researchers often define export flux as the flux leaving the base of the euphotic zone or a specific depth horizon (often 100 m) and are mainly interested in variability in this export flux as well as remineralization at deeper depths (Henson et al., 2011; Marsay et al., 2015; Palevsky and Doney, 2018; Buesseler et al., 2020). While export flux and flux attenuation are important biogeochemical processes to study, our results suggest that shallower sediment trap deployments can illuminate interesting patterns

that may help in understanding the dynamics and vertical structure of the euphotic zone.

Our results show surprisingly high export flux from the upper euphotic zone to the lower euphotic zone (Fig. 8, with the upper and lower euphotic zone defined operationally based on the depth of deployment of our sediment traps, but approximately dividing the euphotic zone equally). In the Argo Basin, sinking particle flux at a depth of ~60-m averaged 8.1 mmol C m^{-2} d^{-1}, which would equate to 27 % of the NPP above this depth horizon. In the more oligotrophic Gulf of Mexico, the proportion of upper euphotic zone NPP exported was even higher, with a flux of 6.4 mmol C m^{-2} d^{-1} equating to 36 % of upper euphotic zone NPP. These results for the Gulf of Mexico are also supported by ^{238}U-^{234}Th disequilibrium results, which suggest that sinking particle flux above the DCM averaged 3.5 mmol C m^{-2} d^{-1} and sinking particle flux beneath the euphotic zone averaged 2.7 mmol C m^{-2} d^{-1} (Stukel et al., 2021). In both regions, the sinking carbon flux from the upper to the lower euphotic zone was approximately equal to the total NPP of the lower euphotic zone. In the Argo Basin 8.1 mmol C m^{-2} d^{-1} sank, compared to lower euphotic zone NPP of 7.8 mmol C m^{-2} d^{-1},
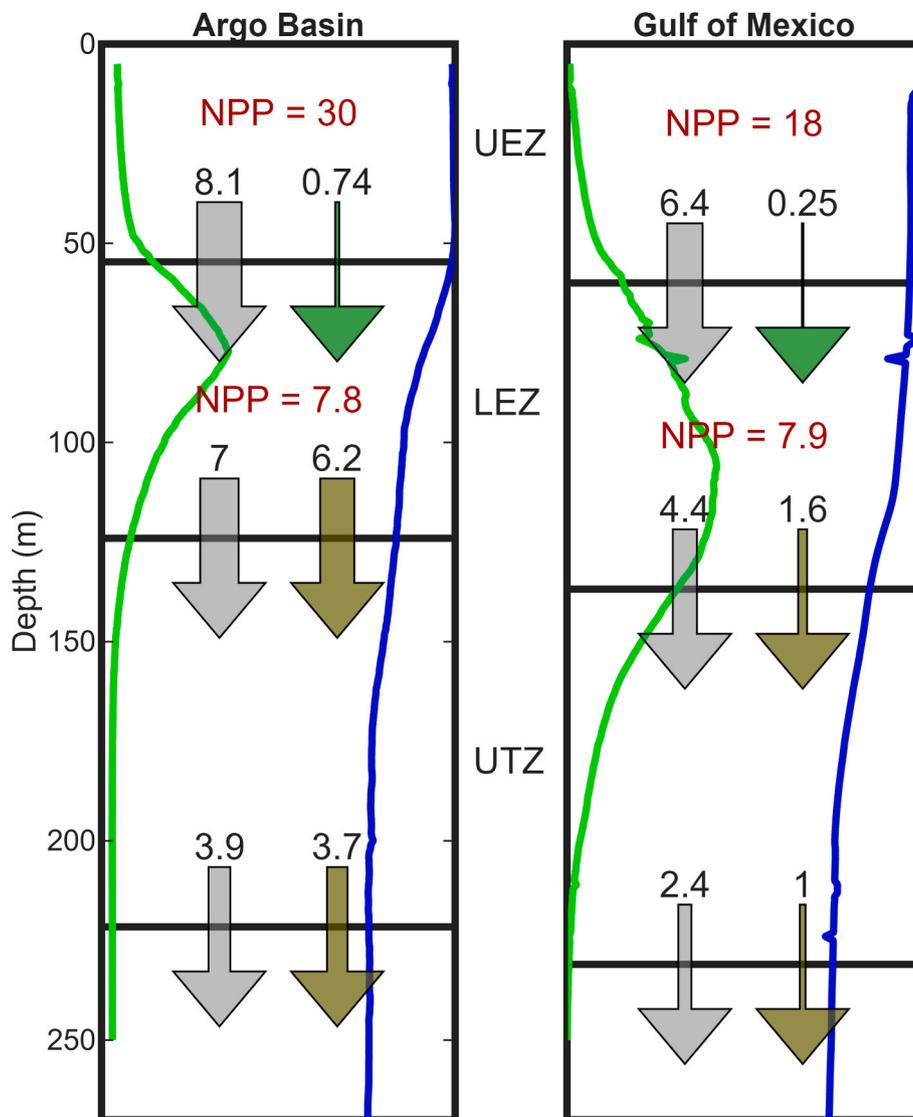

Fig. 8. Average carbon budget for upper and lower euphotic zones (UEZ and LEZ, respectively) and upper twilight zone (UTZ) in the Argo Basin (left) and Gulf of Mexico (right). Gray arrows are sinking particle flux (mmol C m^{-2} d^{-1}). Green arrows are sinking phytoplankton flux from the upper euphotic zone to the lower euphotic zone (mmol C m^{-2} d^{-1}). Brown arrows are sinking herbivore fecal pellet flux (mmol C m^{-2} d^{-1}). Red numbers are net primary production (mmol C m^{-2} d^{-1}). Green profiles are fluorescence and blue profiles are oxygen. Profiles are only shown to highlight vertical structure. For actual values, see Fig. 1 for Argo Basin and Stukel et al. (2021) for Gulf of Mexico. (For interpretation of the references to colour in this figure legend, the reader is referred to the Web version of this article.)

while in the Gulf of Mexico 6.4 mmol C m^{-2} d^{-1} sank and lower euphotic zone NPP was 7.9 mmol C m^{-2} d^{-1}. This suggests that sinking carbon flux must be a quantitatively important carbon input to the lower euphotic zone. Distinct shifts in pigment composition of sinking material (from chlorophyll to phaeopigments) further shows that the lower euphotic zone is a depth stratum in which sinking particles are consumed and re-packaged before they exit the base of the euphotic zone. Using carbon:Chl*a* estimates for the upper euphotic zone (Selph et al., 2021; Yingling et al), we can also get an estimate of phytoplankton carbon flux into the lower euphotic zone. These estimates suggest that 0.74 mmol phytoplankton C m^{-2} d^{-1} exited the upper euphotic zone in the Argo Basin and 0.25 mmol phytoplankton C m^{-2} d^{-1} exited the upper euphotic zone in the GoM. This sinking phytoplankton flux is modest (<10 %) relative to the NPP of the lower euphotic zone. However, even this relatively small flux of phytoplankton may be important when compared to the net growth of phytoplankton in the deep chlorophyll maximum, where protistan grazing often balances (or even exceeds) phytoplankton growth rates, yielding net growth rates <0.1 d^{-1} (Landry et al., 2008, 2021; Selph et al., 2016; Landry et al). The importance of this sinking flux may also be greater when focusing only on the dynamics of large phytoplankton. Although our measurements do not allow us to determine which phytoplankton taxa contributed to the measured chlorophyll flux, it is notable that *Prochlorococcus*, which dominated the phytoplankton biomass during BLOOFINZ-IO and BLOOFINZ-GoM (Selph et al., 2021; Yingling et al), is too small to sink as individual cells. Instead, it is likely that they and other picophytoplankton were concentrated onto appendicularian houses or aggregated into other marine snow prior to sinking. This flux of large, but potentially slowly sinking aggregates (as suggested by UVP6 results), may have been an important nutritional subsidy for mesozooplankton residing in the deep euphotic zone. Indeed, a relatively large component of the mesozooplankton community were grasping, particle-associated copepods including *Oncaea* and *Corycaeus* (Swalethorp et al), suggesting that this sinking carbon may have implications for food-web transfer in the lower euphotic zone.

Our results also suggest that the lower euphotic zone is a region of net particle remineralization. In the Argo Basin, mean sinking carbon flux at the base of the euphotic zone (0.1 % light level) was on average only 86 % of sinking particle flux leaving the upper euphotic zone. In the Gulf of Mexico, the decrease was even stronger with only 69 % of upper euphotic zone export flux exiting the euphotic zone. This implies that the DCM, which has substantial phytoplankton biomass, is nevertheless net heterotrophic. Another way that we can address the question of net heterotrophy vs. net autotrophy is by investigating oxygen profiles. If we make the simplifying assumption that horizontal advection and diffusion are negligible to the water column oxygen budget, then the rate of O$_2$ change follows the equation:

$$\frac{\partial O_2}{\partial t} = -w\frac{\partial O_2}{\partial z} + \frac{\partial}{\partial z}\left(K_z\frac{\partial O_2}{\partial z}\right) + R \qquad \text{Eq. 1}$$

where w is the vertical velocity, K_z is the vertical eddy diffusivity, and R is the net biological production or consumption of oxygen (O$_2$). Vertical velocities are typically weakly downward in oligotrophic regions and this fact, combined with decreasing oxygen with depth near the DCM (Supp. Fig. 4) suggests that vertical advection is a net supply of oxygen to the DCM. Thus, if the advection term is neglected, heterotrophy is underestimated. If we further assume a quasi-steady state and that vertical eddy diffusivity is constant with depth, Eq. (1) becomes:

$$R = -K_z\left(\frac{\partial^2 O_2}{\partial z^2}\right) \qquad \text{Eq. 2}$$

This equation suggests that the community will be net heterotrophic when the second derivative of oxygen is positive. If we integrate this second derivative over the depths of the lower euphotic zone (as defined in Fig. 8), we find that it is slightly positive (Supp. Fig. 4d) and thus

agrees with the hypothesis that the deep euphotic zone is net heterotrophic. Investigating the vertical structure also shows that the second derivative switches from negative to positive at almost exactly the depth of the DCM, which would suggest that the water column switches from net autotrophic to net heterotrophic right at the DCM. We caution, however, that our assumption of no vertical advection likely leads to an underestimation of heterotrophy in the system (as a result of the likely downward average velocities noted above). This would suggest that the switch to heterotrophy might occur at slightly shallower depths than predicted by the second derivative of oxygen. Nevertheless, it is clear that particle consumption and repackaging and net remineralization can begin within the deep euphotic zone and likely shapes the carbon balance of the DCM as well as the characteristics of sinking particles exiting the euphotic zone.

4.3. Conclusions

The Argo Basin is a classic tropical 2-layer stratified, oligotrophic-ocean ecosystem with a low-nutrient low-chlorophyll upper layer and with a strong DCM and nitracline in the lower layer. Sinking organic carbon flux is commensurately low at the base of the euphotic zone, but export efficiency is moderate with EZ-ratios ranging from 0.085 to 0.23, similar to those in the slightly more oligotrophic central Gulf of Mexico. In both of these regions, mean carbon flux out of the upper euphotic zone (i.e., 50–60 m) was higher than particulate carbon export from the base of the euphotic zone (0.1 % light level), suggesting that the deep euphotic zone and DCM is a zone of net remineralization. A distinct shift in the characteristics of sinking particles was also noted between these depth horizons, with sinking chlorophyll flux suggesting that intact phytoplankton were an important component of sinking carbon flux from the upper to lower euphotic zone, while phaeopigments indicated that fecal pellets of herbivorous zooplankton were more important beneath the euphotic zone. Within the twilight zone, flux attenuation was fairly typical for a marine ecosystem, with an average of 62 % of sinking carbon flux penetrating an additional 100 m beneath the euphotic zone in the Argo Basin and 52 % in the Gulf of Mexico. Taken together, our results suggest that export efficiency is greater in these two marginal seas than is typical in open-ocean systems that are equally oligotrophic in terms of other indices of trophic state.

CRediT authorship contribution statement

Michael R. Stukel: Writing – original draft, Investigation, Funding acquisition, Conceptualization. **Tristan Biard:** Writing – review & editing, Resources, Data curation. **Moira Décima:** Writing – review & editing, Investigation, Conceptualization. **Christian K. Fender:** Writing – review & editing, Investigation. **Opeyemi Kehinde:** Writing – review & editing, Investigation. **Thomas B. Kelly:** Writing – review & editing, Investigation. **Sven A. Kranz:** Writing – review & editing, Investigation, Funding acquisition, Conceptualization. **Manon Laget:** Writing – review & editing, Investigation. **Michael R. Landry:** Writing – review & editing, Investigation, Funding acquisition, Conceptualization. **Natalia Yingling:** Writing – review & editing, Investigation.

Declaration of competing interest

The authors declare that they have no known competing financial interests or personal relationships that could have appeared to influence the work reported in this paper.

Acknowledgments

1851347 to M.R.S. and S.A.K. and OCE-1851558 to M.R.L. This study was a part of project EP-46 of the 2nd International Indian Ocean Expedition (IIOE-2). Sampling in the Argo-Rowley Terrace Marine Park was done under Australian Government permit AU-COM2021-520 and permit PA2021-00062-1 issued by the Director of National Parks, Australia.

Appendix A. Supplementary data

Supplementary data to this article can be found online at https://doi.org/10.1016/j.dsr2.2026.105590.

Data availability

Data from this project are available at the Biological and Chemical Oceanography Data Management Office (BCO-DMO) project pages for BLOOFINZ-IO and BLOOFINZ-GoM: https://www.bco-dmo.org/project/819488 and https://www.bco-dmo.org/project/834957. The sediment trap data is available on BCO-DMO as https://doi.org/10.26008/1912/bco-dmo.944902.1 (https://www.bco-dmo.org/dataset/944902). It is also available as Supp. Table 2, although we would refer readers to the BCO-DMO archive as the definitive version.

References

Alldredge, A., 2005. The contribution of discarded appendicularian houses to the flux of particulate organic carbon from oceanic surface waters. In: Gorsky, G., Youngbluth, M., Deibel, D. (Eds.), Response of Marine Ecosystems to Global Change: Ecological Impact of Appendicularians. Archives contemporaines, pp. 309–326.

Andreassen, I.J., Wassmann, P., 1998. Vertical flux of phytoplankton and particulate biogenic matter in the marginal ice zone of the Barents Sea in May 1993. Mar. Ecol. Prog. Ser. 170, 1–14.

Archibald, K.M., Siegel, D.A., Doney, S.C., 2019. Modeling the impact of zooplankton diel vertical migration on the carbon export flux of the biological pump. Glob. Biogeochem. Cycles 33 (2), 181–199.

Bacon, M.P., Cochran, J.K., Hirschberg, D., Hammar, T.R., Fleer, A.P., 1996. Export flux of carbon at the equator during the EqPac time-series cruises estimated from Th-234 measurements. Deep-Sea Res. II 43 (4–6), 1133–1153.

Baker, E.T., Milburn, H.B., Tennant, D.A., 1988. Field assessment of sediment trap efficiency under varying flow conditions. J. Mar. Res. 46 (3), 573–592.

Barber, R.T., Marra, J., Bidigare, R.C., Codispoti, L.A., Halpern, D., Johnson, Z., Latasa, M., Goericke, R., Smith, S.L., 2001. Primary productivity and its regulation in the Arabian Sea during 1995. Deep-Sea Res. II 48 (6–7), 1127–1172.

Bates, N.R., Pequignet, A.C., Sabine, C.L., 2006. Ocean carbon cycling in the Indian Ocean: 1. Spatiotemporal variability of inorganic carbon and air-sea CO_2 gas exchange. Glob. Biogeochem. Cycles 20 (3).

Bianchi, D., Galbraith, E.D., Carozza, D.A., Mislan, K.A.S., Stock, C.A., 2013. Intensification of open-ocean oxygen depletion by vertically migrating animals. Nat. Geosci. 6 (7), 545–548.

Black, E.E., Buesseler, K.O., Pike, S.M., Lam, P.J., 2018. ^{234}Th as a tracer of particulate export and remineralization in the southeastern tropical Pacific. Mar. Chem. 201, 35–50.

Boyd, P.W., Claustre, H., Levy, M., Siegel, D.A., Weber, T., 2019. Multi-faceted particle pumps drive carbon sequestration in the ocean. Nature 568 (7752), 327–335.

Buesseler, K., Ball, L., Andrews, J., Benitez-Nelson, C., Belastock, R., Chai, F., Chao, Y., 1998. Upper ocean export of particulate organic carbon in the Arabian Sea derived from thorium-234. Deep-Sea Res. II 45 (10–11), 2461–2487.

Buesseler, K.O., Antia, A.N., Chen, M., Fowler, S.W., Gardner, W.D., Gustafsson, O., Harada, K., Michaels, A.F., van der Loeff, M.R., Sarin, M., Steinberg, D.K., Trull, T., 2007. An assessment of the use of sediment traps for estimating upper ocean particle fluxes. J. Mar. Res. 65 (3), 345–416.

Buesseler, K.O., Bacon, M.P., Cochran, J.K., Livingston, H.D., 1992. Carbon and nitrogen export during the JGOFS North Atlantic bloom experiment estimated from ^{234}Th:^{238}U disequilibria. Deep Sea Res. 39 (7–8A), 1115–1137.

Buesseler, K.O., Barber, R.T., Dickson, M.-L., Hiscock, M.R., Moore, J.K., Sambrotto, R., 2003. The effect of marginal ice-edge dynamics on production and export in the Southern Ocean along 170 W. Deep-Sea Res. II 50 (3–4), 579–603.

Buesseler, K.O., Boyd, P.W., 2009. Shedding light on processes that control particle export and flux attenuation in the twilight zone of the open ocean. Limnol. Oceanogr. 54 (4), 1210–1232.

Buesseler, K.O., Boyd, P.W., Black, E.E., Siegel, D.A., 2020. Metrics that matter for assessing the ocean biological carbon pump. Proc. Natl. Acad. Sci. U. S. A 117 (18), 9679–9687.

Buesseler, K.O., Lamborg, C., Cai, P., Escoube, R., Johnson, R., Pike, S., Masque, P., McGillicuddy, D., Verdeny, E., 2008. Particle fluxes associated with mesoscale eddies in the Sargasso Sea. Deep-Sea Res. II 55 (10–13), 1426–1444.

Buesseler, K.O., Trull, T.W., Steinber, D.K., Silver, M.W., Siegel, D.A., Saitoh, S.I., Lamborg, C.H., Lam, P.J., Karl, D.M., Jiao, N.Z., Honda, M.C., Elskens, M., Dehairs, F., Brown, S.L., Boyd, P.W., Bishop, J.K.B., Bidigare, R.R., 2008. VERTIGO (VERtical transport in the global ocean): a study of particle sources and flux attenuation in the North Pacific. Deep-Sea Res. II 55 (14–15), 1522–1539.

Carlson, C.A., Ducklow, H.W., Michaels, A.F., 1994. Annual flux of dissolved organic carbon from the euphotic zone in the northwestern Sargasso Sea. Nature 371 (6496), 405–408.

Charette, M.A., Moran, S.B., Bishop, J.K., 1999. 234Th as a tracer of particulate organic carbon export in the subarctic northeast Pacific Ocean. Deep-Sea Res. II 46 (11–12), 2833–2861.

Church, M.J., Lomas, M.W., Muller-Karger, F., 2013. Sea change: charting the course for biogeochemical ocean time-series research in a new millennium. Deep-Sea Res. II 93, 2–15.

Davis, T.L.O., Jenkins, G.P., Young, J.W., 1990. Diel patterns of vertical-distribution in larvae of southern bluefin (Thunnus maccoyii) and other tuna in the East-Indian ocean. Mar. Ecol. Prog. Ser. 59 (1–2), 63–74.

Davison, P.C., Checkley, D.M., Koslow, J.A., Barlow, J., 2013. Carbon export mediated by mesopelagic fishes in the northeast Pacific Ocean. Prog. Oceanogr. 116, 14–30.

Décima, M., Swalethorp, R., Cawley, G., Traboni, C., Davies, C.H., Landry, M.R., this issue. Zooplankton Trophic Processes in the Eastern Indian Ocean Southern Bluefin Tuna Spawning Region. Deep-Sea Res. II.

Domingues, C.M., Maltrud, M.E., Wijffels, S.E., Church, J.A., Tomczak, M., 2007. Simulated lagrangian pathways between the Leeuwin current system and the upper-ocean circulation of the southeast Indian Ocean. Deep-Sea Res. II 54 (8), 797–817.

Eppley, R.W., Peterson, B.J., 1979. Particulate organic matter flux and planktonic new production in the deep ocean. Nature 282 (5740), 677–680.

Fender, C.K., Kelly, T.B., Guidi, L., Ohman, M.D., Smith, M.C., Stukel, M.R., 2019. Investigating particle size-flux relationships and the biological pump across a range of plankton ecosystem states from coastal to oligotrophic. Front. Mar. Sci. 6, 603.

Gerard, T., Lamkin, J., Kelly, T.B., Knapp, A.N., Laiz-Carrión, R., Malca, E., Selph, K.E., Shiroza, A., Shropshire, T.A., Stukel, M.R., Swalethorp, R., Yingling, N., Landry, M.R., 2022. Bluefin Larvae in oligotrophic ocean foodwebs, investigations of nutrients to zooplankton: overview of the BLOOFINZ-gulf of Mexico program. J. Plankton Res. 44 (5), 600–617.

Ghosh, J., Chakraborty, K., Valsala, V., Bhattacharya, T., Ghoshal, P.K., 2024. A review of the Indian Ocean carbon dynamics, acidity, and productivity in a changing environment. Prog. Oceanogr., 103210

Glibert, P.M., Middelburg, J.J., McClelland, J.W., Jake Vander Zanden, M., 2019. Stable isotope tracers: enriching our perspectives and questions on sources, fates, rates, and pathways of major elements in aquatic systems. Limnol. Oceanogr. 64, 950–981.

Guidi, L., Jackson, G.A., Stemmann, L., Miquel, J.C., Picheral, M., Gorsky, G., 2008. Relationship between particle size distribution and flux in the mesopelagic zone. Deep-Sea Res. I 55 (10), 1364–1374.

Hannides, C.C.S., Landry, M.R., Benitez-Nelson, C.R., Styles, R.M., Montoya, J.P., Karl, D.M., 2009. Export stoichiometry and migrant-mediated flux of phosphorus in the North Pacific subtropical Gyre. Deep-Sea Res. I 56 (1), 73–88.

Harrison, W.G., Platt, T., Lewis, M.R., 1987. f-ratio and its relationship to ambient nitrate concentration in coastal waters. J. Plankton Res. 9 (1), 235–248.

Henson, S.A., Laufkötter, C., Leung, S., Giering, S.L.C., Palevsky, H.I., Cavan, E.L., 2022. Uncertain response of ocean biological carbon export in a changing world. Nat. Geosci. 15 (4), 248–254.

Henson, S.A., Sanders, R., Madsen, E., Morris, P.J., Le Moigne, F., Quartly, G.D., 2011. A reduced estimate of the strength of the ocean's biological carbon pump. Geophys. Res. Lett. 38, L04606.

Honjo, S., Dymond, J., Prell, W., Ittekkot, V., 1999. Monsoon-controlled export fluxes to the interior of the Arabian Sea. Deep-Sea Res. II 46 (8–9), 1859–1902.

Hood, R.R., Beckley, L.E., Sarma, V.V.S.S., Vinayachandran, P.N., 2024. The second international indian ocean expedition (IIOE-2): motivating new exploration in a poorly understood ocean basin. Deep-Sea Res. II 6, 105427, 218.

Hood, R.R., Rixen, T., Levy, M., Hansell, D.A., Coles, V.J., Lachkar, Z., 2024. Oxygen, carbon, and pH variability in the Indian Ocean. The Indian Ocean and Its Role in the Global Climate System. Elsevier, pp. 265–291.

Iversen, M.H., Nowald, N., Ploug, H., Jackson, G.A., Fischer, G., 2010. High resolution profiles of vertical particulate organic matter export off cape blanc, Mauritania: degradation processes and ballasting effects. Deep-Sea Res. I 57 (6), 771–784.

Karl, D.M., Letelier, R.M., Bidigare, R.R., Björkman, K.M., Church, M.J., Dore, J.E., White, A.E., 2021. Seasonal-to-decadal scale variability in primary production and particulate matter export at station ALOHA. Prog. Oceanogr. 195, 102563.

Kehinde, O., Bourassa, M., Kranz, S., Landry, M.R., Kelly, T., Stukel, M.R., 2023. Lateral advection of particulate organic matter in the eastern Indian Ocean. J. Geophys. Res., Oceans 128 (5) e2023JC019723.

Kelly, T.B., Knapp, A.N., Landry, M.R., Selph, K.E., Shropshire, T.A., Thomas, R.K., Stukel, M.R., 2021. Lateral advection supports nitrogen export in the oligotrophic open-ocean Gulf of Mexico. Nat. Commun. 12 (1), 3325.

Knapp, A.N., Thomas, R.K., Stukel, M.R., Kelly, T.B., Landry, M.R., Selph, K.E., Malca, E., Gerard, T., Lamkin, J., 2021. Constraining the sources of nitrogen fueling export production in the Gulf of Mexico using nitrogen isotope budgets. J. Plankton Res 44 (5), 692–710.

Knauer, G.A., Martin, J.H., Bruland, K.W., 1979. Fluxes of particulate carbon, nitrogen, and phosphorus in the upper water column of the northeast Pacific. Deep Sea Res. 26 (1), 97–108.

Kranz, S.A., Rose, J., Stukel, M.R., Selph, K.E., Yingling, N., Landry, M.R., 2026. Primary productivity and N$_2$-fixation in the eastern Indian Ocean: bottom-up Support for an Ecologically and Economically Important Ecosystem. Deep-Sea. Res. II 225, 105570. https://doi.org/10.1016/j.dsr2.2025.105570.

Krause, J.W., Brzezinski, M.A., Goericke, R., Landry, M.R., Ohman, M.D., Stukel, M.R., Taylor, A.G., 2015. Variability in diatom contributions to biomass, organic matter production and export across a frontal gradient in the California current ecosystem. J. Geophys. Res., Oceans 120 (2), 1032–1047.

Kumar, S.P., Madhupratap, M., Kumar, M.D., Gauns, M., Muraleedharan, P., Sarma, V., De Souza, S., 2000. Physical control of primary productivity on a seasonal scale in central and eastern Arabian Sea. J. Earth Syst. Sci. 109, 433–441.

Lamborg, C.H., Buesseler, K.O., Valdes, J., Bertrand, C.H., Bidigare, R., Manganini, S., Pike, S., Steinberg, D., Trull, T., Wilson, S., 2008. The flux of bio- and lithogenic material associated with sinking particles in the mesopelagic "twilight zone" of the northwest and North central Pacific Ocean. Deep-Sea Res. II 55 (14–15), 1540–1563.

Landry, M.R., Brown, S.L., Rii, Y.M., Selph, K.E., Bidigare, R.R., Yang, E.J., Simmons, M. P., 2008. Depth-stratified phytoplankton dynamics in cyclone opal, a subtropical mesoscale eddy. Deep-Sea Res. II 55 (10–13), 1348–1359.

Landry, M.R., Ohman, M.D., Goericke, R., Stukel, M.R., Tsyrklevich, K., 2009. Lagrangian studies of phytoplankton growth and grazing relationships in a coastal upwelling ecosystem off Southern California. Prog. Oceanogr. 83, 208–216.

Landry, M.R., Selph, K.E., Stukel, M.R., Swalethorp, R., Kelly, T.B., Beatty, J.L., Quackenbush, C.R., 2021. Microbial food web dynamics in the oceanic Gulf of Mexico. J. Plankton Res.

Landry, M.R., Laiz-Carrión, R., Kranz, S.A., Selph, K.E., Stukel, M.R., Malca, E., Die, D., Beckley, L.E., Décima, M., Swalethorp, R., Quintanilla, J.M., Yingling, N., Davies, C. H., Traboni, C., Borrego-Santos, R., Goes, J.I., de Souza, J., Romero-Fernandez, R., Grazia Pennino, M., Kim, L.E., Kehinde, O., Lampe, R.H., Allen, A.E., Kelly, T.B., Muhling, B.A., Gu, S., Cassar, N., Laget, M., Biard, T., Liu, H., Hong Io, K., Shiroza, A., Cawley, G.F., Fender, C.K., Rose, J.M., Jivanjee, A., Matisons, L., 2022. This issue-a. Overview of BLOOFINZ/INDITUN Investigations of the Southern Bluefin Spawning Region off Northwest Australia, January-March 2022. Deep-Sea Res. II. https://doi.org/10.1016/j.dsr2.2025.105564.

Landry, M.R., Stukel, M.R., Yingling, N., Selph, K.E., Kranz, S.A., Fender, C.K., Swalethorp, R., Bhabu, R., This issue-b. Microbial Food Web Dynamics in Tropical Waters of the Bluefin Tuna Spawning Region off Northwestern Australia. Deep-Sea Res. II.

Laufkötter, C., Vogt, M., Gruber, N., Aumont, O., Bopp, L., Doney, S.C., Dunne, J.P., Hauck, J., John, J.G., Lima, I.D., Seferian, R., Völker, C., 2016. Projected decreases in future marine export production: the role of the carbon flux through the upper ocean ecosystem. Biogeosciences 13 (13), 4023–4047.

Laws, E.A., D'Sa, E., Naik, P., 2011. Simple equations to estimate ratios of new or export production to total production from satellite-derived estimates of sea surface temperature and primary production. Limnol Oceanogr. Methods 9, 593–601.

Lee, C., Murray, D., Barber, R., Buesseler, K., Dymond, J., Hedges, J., Honjo, S., Manganini, S., Marra, J., Moser, C., 1998. Particulate organic carbon fluxes: compilation of results from the 1995 US JGOFS Arabian Sea process study: the Arabian Sea carbon flux group. Deep-Sea Res. II 45 (10–11), 2489–2501.

Lomas, M.W., Bates, N.R., Johnson, R.J., Knap, A.H., Steinberg, D.K., Carlson, C.A., 2013. Two decades and counting: 24-years of sustained open ocean biogeochemical measurements in the Sargasso Sea. Deep-Sea Res. II 93, 16–32.

Lombard, F., Kiorboe, T., 2010. Marine snow originating from appendicularian houses: age-dependent settling characteristics. Deep-Sea Res. I 57 (10), 1304–1313.

Longhurst, A.R., Bedo, A.W., Harrison, W.G., Head, E.J.H., Sameoto, D.D., 1990. Vertical flux of respiratory carbon by oceanic diel migrant biota. Deep Sea Res. 37 (4), 685–694.

Marra, J., Barber, R.T., 2005. Primary productivity in the Arabian Sea: a synthesis of JGOFS data. Prog. Oceanogr. 65 (2–4), 159–175.

Marsay, C.M., Sanders, R.J., Henson, S.A., Pabortsava, K., Achterberg, E.P., Lampitt, R.S., 2015. Attenuation of sinking particulate organic carbon flux through the mesopelagic ocean. Proc. Natl. Acad. Sci. U. S. A 112 (4), 1089–1094.

Martin, J.H., Knauer, G.A., Karl, D.M., Broenkow, W.W., 1987. Vertex: carbon cycling in the northeast Pacific. Deep Sea Res. 34 (2), 267–285.

McConnaughey, T., McRoy, C., 1979. Food-web structure and the fractionation of carbon isotopes in the Bering Sea. Mar. Biol. 53 (3), 257–262.

McDonnell, A.M.P., Buesseler, K.O., 2010. Variability in the average sinking velocity of marine particles. Limnol. Oceanogr. 55 (5), 2085–2096.

Menden-Deuer, S., Lessard, E.J., 2000. Carbon to volume relationships for dinoflagellates, diatoms, and other protist plankton. Limnol. Oceanogr. 45 (3), 569–579.

Michaels, A.F., Silver, M.W., 1988. Primary production, sinking fluxes and the microbial food web. Deep Sea Res. 35 (4), 473–490.

Nowicki, M., DeVries, T., Siegel, D.A., 2022. Quantifying the carbon export and sequestration pathways of the ocean's biological carbon pump. Glob. Biogeochem. Cycles 36 (3) e2021GB007083.

Olli, K., Riser, C.W., Wassmann, P., Ratkova, T., Arashkevich, E., Pasternak, A., 2001. Vertical flux of biogenic matter during a Lagrangian study off the NW Spanish continental margin. Prog. Oceanogr. 51 (2–4), 443–466.

Omand, M.M., D'Asaro, E.A., Lee, C.M., Perry, M.J., Briggs, N., Cetinić, I., Mahadevan, A., 2015. Eddy-driven subduction exports particulate organic carbon from the spring bloom. Science 348 (6231), 222–225.

Palevsky, H.I., Doney, S.C., 2018. How choice of depth horizon influences the estimated spatial patterns and global magnitude of ocean carbon export flux. Geophys. Res. Lett.

Passow, U., Shipe, R.F., Murray, A., Pak, D.K., Brzezinski, M.A., Alldredge, A.L., 2001. The origin of transparent exopolymer particles (TEP) and their role in the sedimentation of particulate matter. Cont. Shelf Res. 21 (4), 327–346.

Picheral, M., Catalano, C., Brousseau, D., Claustre, H., Coppola, L., Leymarie, E., Coindat, J., Dias, F., Fevre, S., Guidi, L., 2022. The Underwater vision profiler 6: an imaging sensor of particle size spectra and plankton, for autonomous and cabled platforms. Limnol Oceanogr. Methods 20 (2), 115–129.

Post, D.M., 2002. Using stable isotopes to estimate trophic position: models, methods, and assumptions. Ecology 83 (3), 703–718.

Puigcorbé, V., Roca-Martí, M., Masqué, P., Benitez-Nelson, C., Rutgers van der Loeff, M., Bracher, A., Moreau, S., 2017. Latitudinal distributions of particulate carbon export across the North Western Atlantic Ocean. Deep-Sea Res. I 129 (Suppl. C), 116–130.

Rixen, T., Gaye, B., Emeis, K.-C., 2019. The monsoon, carbon fluxes, and the organic carbon pump in the northern Indian Ocean. Prog. Oceanogr. 175, 24–39.

Sarma, V.V.S.S., Swathi, P.S., Kumar, M.D., Prasannakumar, S., Bhattathiri, P.M.A., Madhupratap, M., Ramaswamy, V., Sarin, M.M., Gauns, M., Ramaiah, N., Sardessai, S., de Sousa, S.N., 2003. Carbon budget in the eastern and central Arabian Sea: an Indian JGOFS synthesis. Glob. Biogeochem. Cycles 17 (4), 1102.

Selph, K.E., Landry, M.R., Taylor, A.G., Gutierrez-Rodriguez, A., Stukel, M.R., Wokuluk, J., Pasulka, A., 2016. Phytoplankton production and taxon-specific growth rates in the Costa Rica dome. J. Plankton Res. 38 (2), 199–215.

Selph, K.E., Swalethorp, R., Stukel, M.R., Kelly, T.B., Knapp, A.N., Fleming, K., Hernandez, T., Landry, M.R., 2021. Phytoplankton community composition and biomass in the oligotrophic Gulf of Mexico. J. Plankton Res.

Siegel, D.A., Buesseler, K.O., Doney, S.C., Sailley, S.F., Behrenfeld, M.J., Boyd, P.W., 2014. Global assessment of ocean carbon export by combining satellite obervations and food-web models. Glob. Biogeochem. Cycles 28 (3), 181–196.

Siegel, D.A., Fields, E., Buesseler, K.O., 2008. A bottom-up view of the biological pump: modeling source funnels above ocean sediment traps. Deep-Sea Res. I 55 (1), 108–127.

Smayda, T.J., 1970. The suspension and sinking of phytoplankton in the sea. Oceanogr. Mar. Biol. Annu. Rev. 8, 353–414.

Smith, K.L., Ruhl, H.A., Huffard, C.L., Messié, M., Kahru, M., 2018. Episodic organic carbon fluxes from surface ocean to abyssal depths during long-term monitoring in NE Pacific. Proc. Natl. Acad. Sci. U. S. A 115 (48), 12235–12240.

Sprintall, J., Biastoch, A., Gruenburg, L.K., Phillips, H.E., 2024. Oceanic basin connections. The Indian Ocean and its Role in the Global Climate System. Elsevier, pp. 205–227.

Steinberg, D.K., Carlson, C.A., Bates, N.R., Goldthwait, S.A., Madin, L.P., Michaels, A.F., 2000. Zooplankton vertical migration and the active transport of dissolved organic and inorganic carbon in the Sargasso Sea. Deep-Sea Res. I 47 (1), 137–158.

Steinberg, D.K., Landry, M.R., 2017. Zooplankton and the ocean carbon cycle. Ann. Rev. Mar. Sci 9, 413–444.

Stukel, M.R., Aluwihare, L.I., Barbeau, K.A., Chekalyuk, A.M., Goericke, R., Miller, A.J., Ohman, M.D., Ruacho, A., Song, H., Stephens, B.M., Landry, M.R., 2017. Mesoscale ocean fronts enhance carbon export due to gravitational sinking and subduction. Proc. Natl. Acad. Sci. U. S. A 114 (6), 1252–1257.

Stukel, M.R., Barbeau, K.A., 2020. Investigating the nutrient landscape in a coastal upwelling region and its relationship to the biological carbon pump. Geophys. Res. Lett. 47 (6) e2020GL087351.

Stukel, M.R., Benitez-Nelson, C., Décima, M., Taylor, A.G., Buchwald, C., Landry, M.R., 2016. The biological pump in the Costa Rica dome: an open ocean upwelling system with high new production and low export. J. Plankton Res. 38 (2), 348–365.

Stukel, M.R., Décima, M., Kelly, T.B., Landry, M.R., Nodder, S.D., Ohman, M.D., Selph, K. E., Yingling, N., 2024. Relationships between plankton size spectra, net primary production, and the biological carbon pump. Glob. Biogeochem. Cycles 38 (4) e2023GB007994.

Stukel, M.R., Décima, M., Landry, M.R., 2022. Quantifying biological carbon pump pathways with a data-constrained mechanistic model ensemble approach. Biogeosciences 19 (15), 3595–3624.

Stukel, M.R., Gerard, T., Kelly, T.B., Knapp, A.N., Laiz-Carrión, R., Lamkin, J., Landry, M. R., Malca, E., Shiroza, A.A.S.T., Selph, K.E., Swalethorp, R., 2022. Plankton food webs of the Gulf of Mexico spawning grounds of Atlantic Bluefin tuna. J. Plankton Res. 44 (5), 763–781.

Stukel, M.R., Irving, J.P., Kelly, T.B., Ohman, M.D., Fender, C.K., Yingling, N., 2023. Carbon sequestration by multiple biological pump pathways in a coastal upwelling biome. Nat. Commun. 14 (1), 2024.

Stukel, M.R., Kelly, T.B., Landry, M.R., Selph, K.E., Swalethorp, R., 2021. Sinking carbon, nitrogen, and pigment flux within and beneath the euphotic zone in the oligotrophic, open-ocean Gulf of Mexico. J. Plankton Res. 44 (5), 711–727.

Stukel, M.R., Landry, M.R., Fender, C.K., Kranz, S.A., Laiz-Carrión, R., Malca, E., Shiroza, A., Selph, K.E., Swalethorp, R., Yingling, N., This Issue. A Comparative Ecosystem Analysis of Contrasting Oligotrophic Spawning Grounds of Bluefin Tuna.

Subha Anand, S., Rengarajan, R., Sarma, V., 2018. 234Th-Based carbon export flux along the Indian GEOTRACES GI02 section in the Arabian Sea and the Indian Ocean. Glob. Biogeochem. Cycles 32 (3), 417–436.

Swalethorp, R., Malca, E., Shiroza, A., Kim, L., Decima, M., Quintanilla, J.M., Borrego-Santos, R., Davies, C.H., Die, D., Beckley, L.E., Traboni, C., Cawley, G., Walsh, K., Landry, M.R., Laiz-Carrión, R., This issue. Selective feeding in Southern bluefin tuna (Thunnus maccoyii) larvae in the argo basin, Eastern Indian Ocean Spawning Ground. Deep-Sea Res. II.

Turner, J.T., 2015. Zooplankton fecal pellets, marine snow, phytodetritus and the ocean's biological pump. Prog. Oceanogr. 130 (0), 205–248.

Wakeham, S.G., Lee, C., 2019. Limits of our knowledge, part 2: selected frontiers in marine organic biogeochemistry. Mar. Chem.

Yingling, N., Kelly, T.B., Selph, K.E., Landry, M.R., Knapp, A.N., Kranz, S.A., Stukel, M.R., 2022. Taxon-specific phytoplankton growth, nutrient limitation, and light limitation in the oligotrophic Gulf of Mexico. J. Plankton Res. 44 (5), 656–676.

Yingling, N., Selph, K.E., Landry, M.R., Kranz, S.A., Johnson, M., Stukel, M.R., This issue. Phytoplankton nutrient uptake, abundance, biomass and community composition in the oligotrophic argo basin, Indian Ocean. Deep-Sea Res. II.